Deep Fire Topology: Understanding the role of landscape spatial patterns in wildfire susceptibility

Cristobal Pais
UC Berkeley, IEOR dept.
cpaismz@berkeley.edu

Alejandro Miranda
Universidad de La Frontera
University of Chile, CR^2
mirandac.alejandro@gmail.com

Jaime Carrasco
University of Chile, ISCI.
jaimecarrasco@ug.uchile.cl

Zuo-Jun Max Shen
UC Berkeley, IEOR dept.
maxshen@berkeley.edu

Abstract

Increasing wildfire activity across the globe has become an urgent issue with enormous ecological and social impacts. While there is evidence that landscape topology affects fire growth, no study has yet reported its potential influence on fire ignition. This study proposes a deep learning framework focused on understanding the impact of different landscape topologies on the ignition of a wildfire and the rationale behind these results. Our model achieves an accuracy of above 90% in fire occurrence prediction, detection, and classification of risky areas by only exploiting topological pattern information from 17,579 landscapes. This study reveals the strong potential of landscape topology in wildfire occurrence prediction and its implications for similar research. The proposed methodology can be applied to multiple fields/studies to understand and capture the role and impact of different topological features and their interactions.

Introduction

An open and growing challenge is the increase in wildfire occurrences across the globe because of its enormous ecological and social impacts, along with its devastating effects on biodiversity and greenhouse gas emissions [14]. Recent megafires in California, Australia, Greece, Chile, Brazil, and Portugal, among other countries, reveal the need for new approaches to understand them [16]. In the context of Deep Learning (DL) models in this field, models trained for fire detection [20], wildfire spread prediction [9], and fire susceptibility mapping [23] are some examples found in the literature [11]. The study of fire occurrence or fire risk focuses on measuring the chance that a fire might start. Although some studies have reported that landscape topology affects fire growth [5], no study has reported the effect of landscape topology on fire occurrence. Previous studies have considered risk factors derived from weather, danger indices, physiography, land-cover, or socioeconomic variables [4], which, in general, are one-dimensional numerical or categorical variables. However, we have not found any modeling efforts that try to capture landscape topology as a predictor of fire risk, thus necessitating the present study.

In general, capturing topological aspects is more complex than constructing a one-dimensional variable such as temperature, topography, and socioeconomic or landscape composition in an area of interest. However, the spatial configuration of these elements may influence and modify fire regimes [1]. Land-cover data represent the basic information for landscape analysis at a pixel level of the primary land uses in a geographically delimited territory. This two-dimensional representation of the landscape also captures an intrinsic relationship between adjacency and connectivity of its

Tackling Climate Change with Machine Learning workshop at NeurIPS 2020.

components, which can be studied to understand landscape phenomena and complex patterns and processes, thanks to the increasing availability of global data at a high and medium spatial resolution.

In this paper, we introduce deep fire topology (DFT), a comprehensive framework (available as an open-source software) for landscape topology analysis by training a DL model while focusing on understanding the rationale behind the results, to assess images associated with different response variables in ecological applications. We present an application on the landscape ecology of fire risk to evaluate the land-cover topology as a predictor of the fire occurrence probability. We use a convolutional neural network (CNN) model without considering additional information such as population density or weather features, which are generally used as variables [4]. We use a supervised learning approach where land-cover images are labeled as fire or no-fire, representing the presence/absence of an ignition. We also open the DL black box focusing on results interpretability.

Methods

Data. We tested our approach using data from south-central Chile (see Appendix). It includes eight administrative regions (212,000 km2), corresponding to 28% of the country, which accounts for 98.5% of the historical fire occurrence [6]. We used a subset (January 2013 to December 2015) of the public database of wildfires provided by the Chilean Forest Service that includes the ignition point for each fire from 0.01 ha of burned area. We used this temporal window because to use the most accurate land-cover map of the country [24]. These land-cover data are in a raster grid that includes ten classes: croplands, native forest, forest plantation, grasslands, shrublands, wetlands, water bodies, impervious surfaces, barren land, and snow/ice. In this study area, the impervious surface is represented mainly by urban and industrial infrastructure.

The association of fire point pattern with land-cover was carried out in the Google Earth Engine (GEE). From these areas, we extract a buffered area with a radius of 560 m centered in randomly generated points. Accounting for imbalance, we eliminate landscapes with a low proportion of fire-prone classes, deleting a landscape with more than 30% of its pixels being non-flammable. We associate each 1 km2 landscape with the fire occurrence frequency in the 2013–2015 period. The final dataset comprises 17,579 32 x 32 images. We use the synthetic minority over-sampling technique (SMOTE) [2] to account for imbalanced data in the training set.

Model. Following the VGGNet architecture [19], our net stacks multiple (5) 3 × 3 filters to extract topological features on top of each other before performing max-pooling operations. Depthwise separable convolutions [3] are used decrease the model size. We include batch normalization [10] and dropout [22] layers after each block to improve convergence and avoid over-fitting. We performed an exhaustive grid search of the most relevant hyper-parameters of the model (learning rate, batch size, and number of layers). We use data augmentation algorithms (rotation, zoom, and shifts) to improve the model generalization. To further understand the impact of topological configurations, the role of discontinuities within the landscape, and the proportion of different land-covers in fire susceptiblity, we implement GradCAM [17], guided backpropagation [18], and guided GradCAM. The analysis of these outputs provides insights into the information that the model focuses on to predict the most likely class of a sample and obtain relevant local statistics.

Results

DFT predicted with an accuracy of 91.85% in the validation (25%) set after 50 training epochs (area under the curve (AUC) = 0.98; specificity = 0.91, sensitivity = 0.96). A similar performance was obtained when deploying the trained model over the entire dataset (AUC = 0.98, specificity = 0.95, sensitivity = 0.95, and accuracy = 92.4%). As expected, the inclusion of SMOTE and data augmentation techniques had a strong impact on the model performance, significantly boosting the original results (accuracy = 82.7%, sensitivity = 0.65, and AUC = 0.61) and improving the convergence of the algorithm.

To understand the results of the model, we ordered the observations by their predicted probability of ignition (P_i), splitting them into three classes: high-risk ($P_i \leq 0.7$), medium-risk ($0.3 \leq P_i < 0.7$), and low-risk ($P_i < 0.3$). From the results (Fig. 2), we observe that the performance of the model across all categories and metrics is stable, obtaining the best overall performance with the high-risk

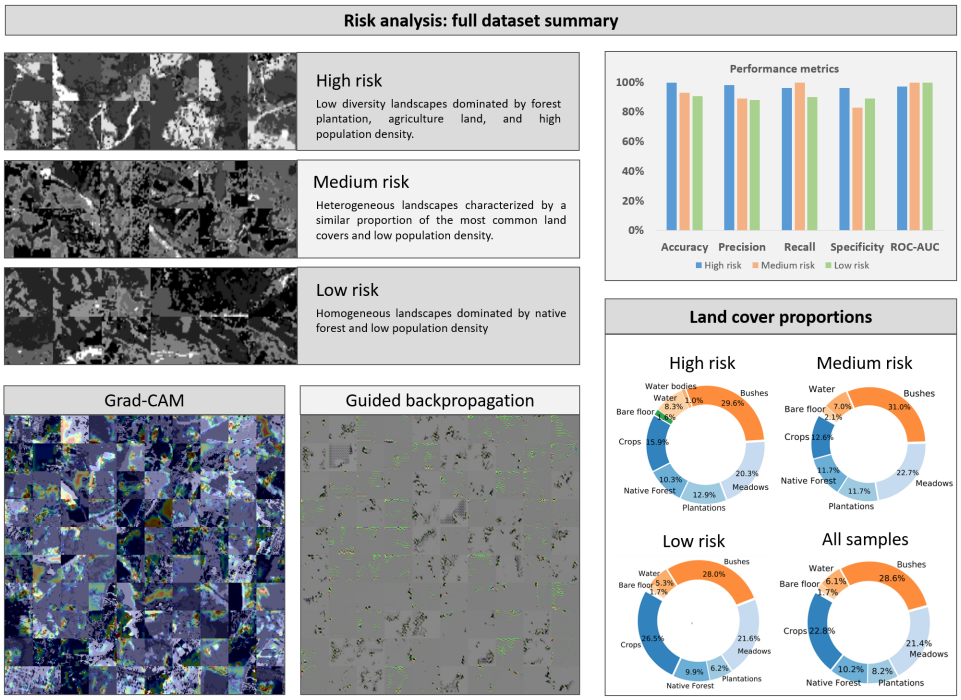

Figure 1: Summary results obtained for the entire dataset divided into three risk categories defined from the predicted fire ignition probability. Performance metrics of the classification algorithm and land-cover proportions are shown on the right panels. Resulting attention maps from one hundred randomly selected samples using GradCAM and guided backpropagation (BP) are also shown.

group (accuracy = 100%). We observe clear patterns from the attention maps, focusing on the interaction, adjacency, total area covered, number of land-cover discontinuities, like dense urban areas with flammable grasslands or large areas with continuous flammable covers, to determine wildfire ignition risk (Appendix Table 1; Fig. 4). The classified images were filtered using the masks generated from the attention maps, allowing us to obtain zonal statistics of the most relevant areas. As shown in Fig. 4, we calculate the zonal statistics at four levels depending on the heatmap density, starting from the complete attention map to its densest area (red hotspots). The results for the entire dataset are summarized in Table 1 and Fig.2, observing significant differences between all categories.

DFT predicts the risk category accurately, and the results showed the different landscape metrics to understand why each image is classified as high, medium, or low-risk (Figs. 1 and 2). More than 95% of wildfires in Chile are human-caused fires [6]. Therefore, fire frequency is closely related to zones with a human footprint, such as cities or other highly human-populated areas and roads, and agricultural or forest plantation industry [7, 13]. Considering this evidence, we classified high-risk landscapes as those with land-cover dominated by industrial activities, such as forest plantation or agricultural activities, with a high population density represented by urban areas and high road density. Conversely, low-risk landscapes are those with a homogeneous native forests land-cover and low human population density. The results from DFT coincided with these criteria.

Moreover, the model classified 97% of the images in the expected risk category. Forest plantation cover increases from 6% (low-risk) to 13% in high-risk landscapes, in agreement with the findings in [13]; however, these landscapes have a relatively stable proportion of the other land-cover types. Another differentiating pattern is the average number of patches in the risk categories following an increasing trend from 88 (low-risk) to 118 (high-risk) components. The number of patches is not only a proxy of landscape fragmentation, but also of the landscape heterogeneity. Therefore, the interpretation must be cautious [8], and may be caused by different landscape processes depending on the predominant land-cover types. Users must have a prior knowledge of the landscape processes and dynamics for a correct interpretation of the models based on machine learning algorithms [15].

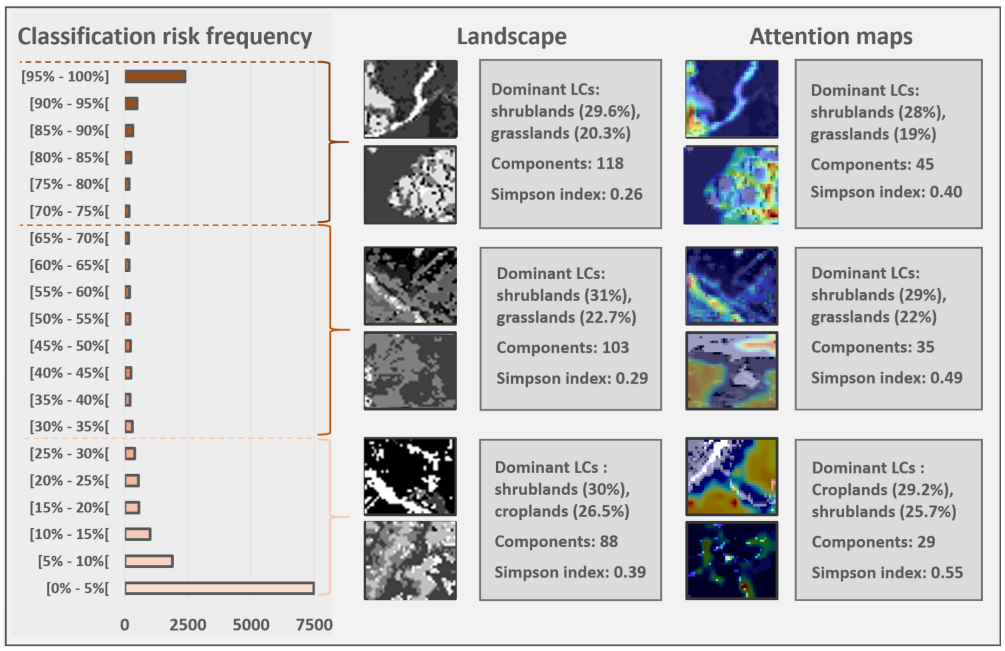

Figure 2: Risk predictions and characterization using activation maps. Horizontal bars indicate the number of observations at different intervals representing the positive class probability. Samples are then separated into three categories and characterized by calculating zonal statistics within the attention maps hotspots. Zonal statistics are obtained by focusing on high-density areas of the map to characterize the learning process of the classification model based on the detected topological structures and interaction between multiple land-covers.

Attention maps point out what specific patterns, interactions, or land-cover classes are critical for image interpretation and categorization. Despite the previously mentioned differences between the risk categories identified by DFT (Fig. 2), the landscape metrics that compare the complete image against the hottest attention map areas show clear differences between the categories. They showed that more fragmented but less diverse landscapes are classified as high risk, which is reflected in more components and a lower Simpson's index [12]. These differences help improve the identification of the most relevant patterns in a landscape, that affect the propensity of fire ignition, having the same trend in both the complete image and the hot spots. The results agree with certain human-caused fires, with fire ignition mainly associated with a highly fragmented wildland–urban interface [21].

The attention maps also provide insights of which land-cover requires more attention to classify the images in the risk categories. In Table 2 and Fig. 5, we show that different layers pay attention to different land-cover types. In the original image, the dominant land-cover for the high-risk (HR) image is forest plantation (47%); however, for layer 0, DFT focused on non-vegetated areas. The areas represented by urban land-covers and roads dominate the hottest pixels by 38% and the forest plantation is only 21%. The attention paid by DFT in non-vegetated areas even increases when filtering the landscape by the 75% hot spot, covering 73% of the hottest pixels. Layer 8 still paid more attention to non-vegetated areas but in combination with grassland, as it is the second dominant land-cover among the hottest pixels (75% threshold). Deeper in the net, DFT focused on the effect of forest plantations, showing patterns similar to some recent findings [7, 13]. The combined layers can provide a general overview of the interaction among land-covers that boosts the propensity of fire ignition as well as observing where the most critical interactions occur.

Conclusions

The interaction between land-covers, continuity, and heterogeneity of the landscape concerning fire risk assessment is empirically evaluated for the first time using DL and the proposed topological interpretation. In the field of forest fire protection, this novel methodology is a step toward landscape

planning under fire risk, avoiding dangerous land-cover spatial distribution, heterogeneity, and interactions. In general, however, it could be an essential development in landscape pattern and process interpretation in a broader sense for different ecological disciplines. The proposed methodology adequately assesses the susceptibility to fire occurrence, using only information on land-cover.

References

[1] Ane A Alencar et al. "Landscape fragmentation, severe drought, and the new Amazon forest fire regime". In: *Ecological applications* 25.6 (2015), pp. 1493–1505.

[2] Nitesh V Chawla et al. "SMOTE: synthetic minority over-sampling technique". In: *Journal of artificial intelligence research* 16 (2002), pp. 321–357.

[3] François Chollet. "Xception: Deep learning with depthwise separable convolutions". In: *Proceedings of the IEEE conference on computer vision and pattern recognition*. 2017, pp. 1251–1258.

[4] Andrea De Montis et al. "Landscape fragmentation in Mediterranean Europe: A comparative approach". In: *Land use policy* 64 (2017), pp. 83–94.

[5] Mark A Finney. "Design of regular landscape fuel treatment patterns for modifying fire growth and behavior". In: *Forest Science* 47.2 (2001), pp. 219–228.

[6] Mauro E González et al. "The 2010–2015 Megadrought and its influence on the fire regime in central and south-central Chile". In: *Ecosphere* 9.8 (2018), e02300.

[7] Mauro E González et al. "The 2010–2015 Megadrought and its influence on the fire regime in central and south-central Chile". In: *Ecosphere* 9.8 (2018), e02300.

[8] Eric J Gustafson. "How has the state-of-the-art for quantification of landscape pattern advanced in the twenty-first century?" In: *Landscape Ecology* 34.9 (2019), pp. 2065–2072.

[9] Jonathan L Hodges and Brian Y Lattimer. "Wildland Fire Spread Modeling Using Convolutional Neural Networks". In: *Fire Technology* 55.6 (2019), pp. 2115–2142.

[10] Sergey Ioffe and Christian Szegedy. "Batch normalization: Accelerating deep network training by reducing internal covariate shift". In: *arXiv preprint arXiv:1502.03167* (2015).

[11] Piyush Jain et al. "A review of machine learning applications in wildfire science and management". In: *arXiv preprint arXiv:2003.00646* (2020).

[12] Kevin McGarigal. *FRAGSTATS: spatial pattern analysis program for quantifying landscape structure*. Vol. 351. US Department of Agriculture, Forest Service, Pacific Northwest Research Station, 1995.

[13] David B McWethy et al. "Landscape drivers of recent fire activity (2001-2017) in south-central Chile". In: *PLoS one* 13.8 (2018), e0201195.

[14] Max A Moritz et al. "Learning to coexist with wildfire". In: *Nature* 515.7525 (2014), p. 58.

[15] Raechel A Portelli. "Don't throw the baby out with the bathwater: reappreciating the dynamic relationship between humans, machines, and landscape images". In: *Landscape Ecology* (2020), pp. 1–8.

[16] Volker C Radeloff et al. "Rapid growth of the US wildland-urban interface raises wildfire risk". In: *Proceedings of the National Academy of Sciences* 115.13 (2018), pp. 3314–3319.

[17] Ramprasaath R Selvaraju et al. "Grad-cam: Visual explanations from deep networks via gradient-based localization". In: *Proceedings of the IEEE international conference on computer vision*. 2017, pp. 618–626.

[18] Avanti Shrikumar, Peyton Greenside, and Anshul Kundaje. "Learning important features through propagating activation differences". In: *Proceedings of the 34th International Conference on Machine Learning-Volume 70*. JMLR. org. 2017, pp. 3145–3153.

[19] Karen Simonyan and Andrew Zisserman. "Very deep convolutional networks for large-scale image recognition". In: *arXiv preprint arXiv:1409.1556* (2014).

[20] Maria João Sousa, Alexandra Moutinho, and Miguel Almeida. "Wildfire detection using transfer learning on augmented datasets". In: *Expert Systems with Applications* 142 (2020), p. 112975.

[21] Alexandra D Syphard and Jon E Keeley. "Location, timing and extent of wildfire vary by cause of ignition". In: *International Journal of Wildland Fire* 24.1 (2015), pp. 37–47.

[22] Wojciech Zaremba, Ilya Sutskever, and Oriol Vinyals. "Recurrent neural network regularization". In: *arXiv preprint arXiv:1409.2329* (2014).

[23] Guoli Zhang, Ming Wang, and Kai Liu. “Forest Fire Susceptibility Modeling Using a Convolutional Neural Network for Yunnan Province of China”. In: *International Journal of Disaster Risk Science* 10.3 (2019), pp. 386–403.

[24] Yuanyuan Zhao et al. “Detailed dynamic land cover mapping of Chile: Accuracy improvement by integrating multi-temporal data”. In: *Remote Sensing of Environment* 183 (2016), pp. 170–185.

Appendix

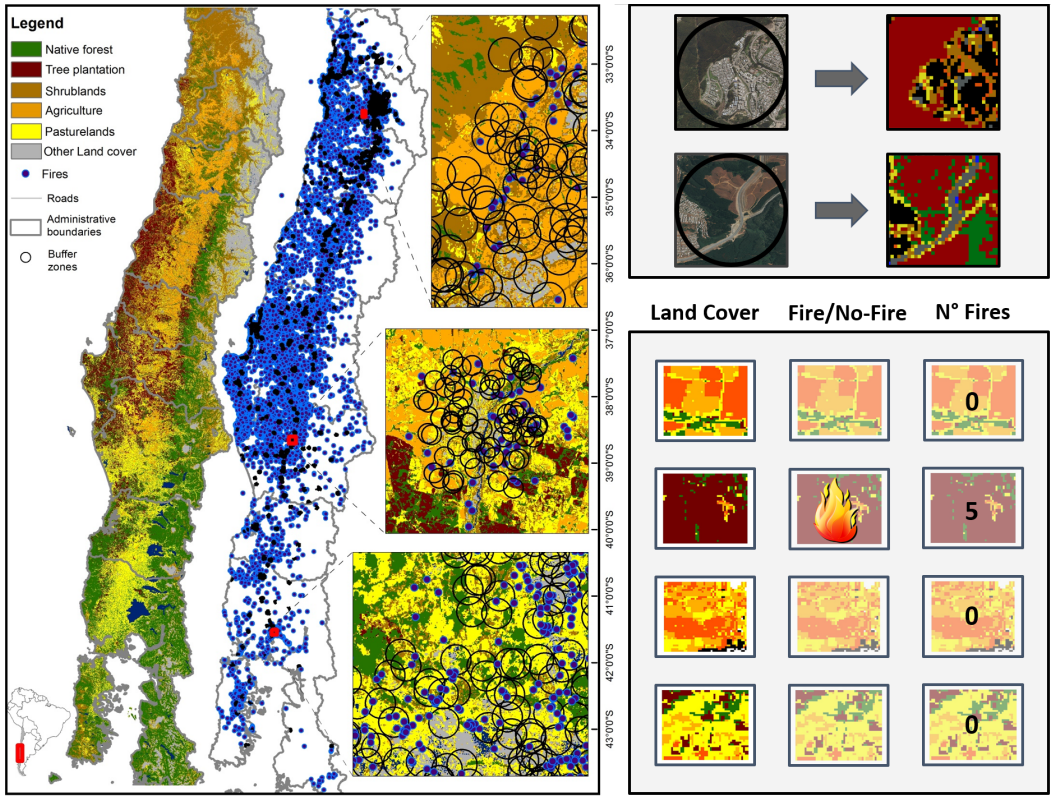

Figure 3: Case study data. Ignition points of wildfires distributed along the national territory of Chile are highlighted (A). A buffer is generated for each point (B) to extract a rectangular land-cover image centered at the ignition coordinates (C).

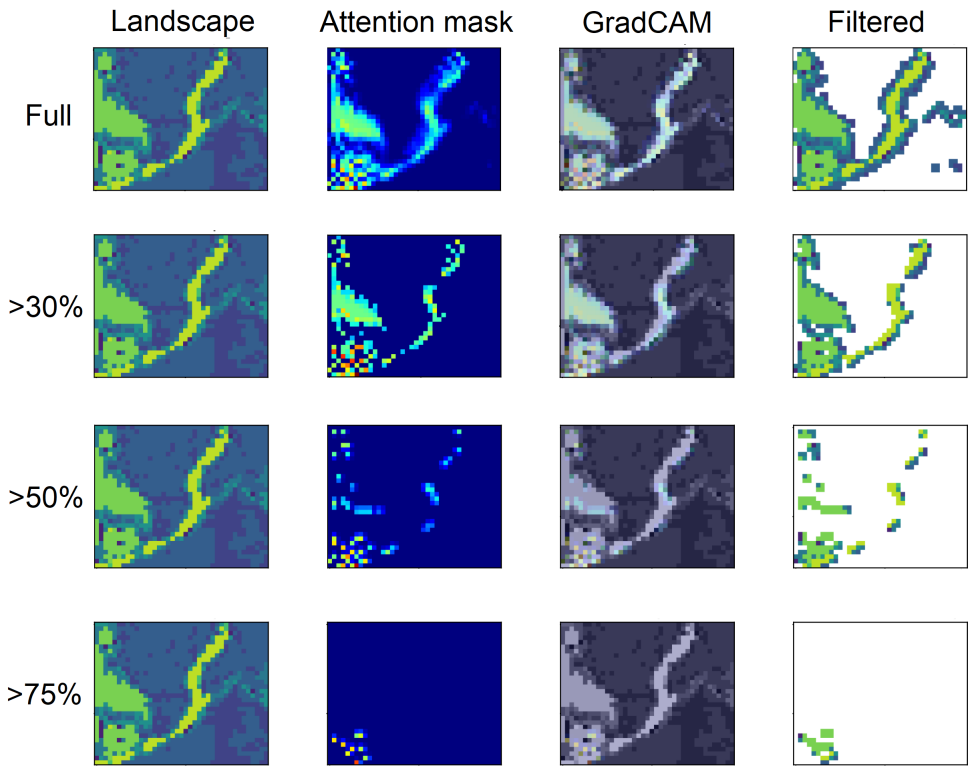

Figure 4: Filtered landscapes using different attention levels (full map, top 30%, 50%, and 75% of the densest areas). Attention masks are calculated at different density thresholds to filter the original landscapes, focusing the analysis on the densest sections of the attention maps. Red to blue color represent a gradient from the most to the least relevant zones to classify an image as a positive case.

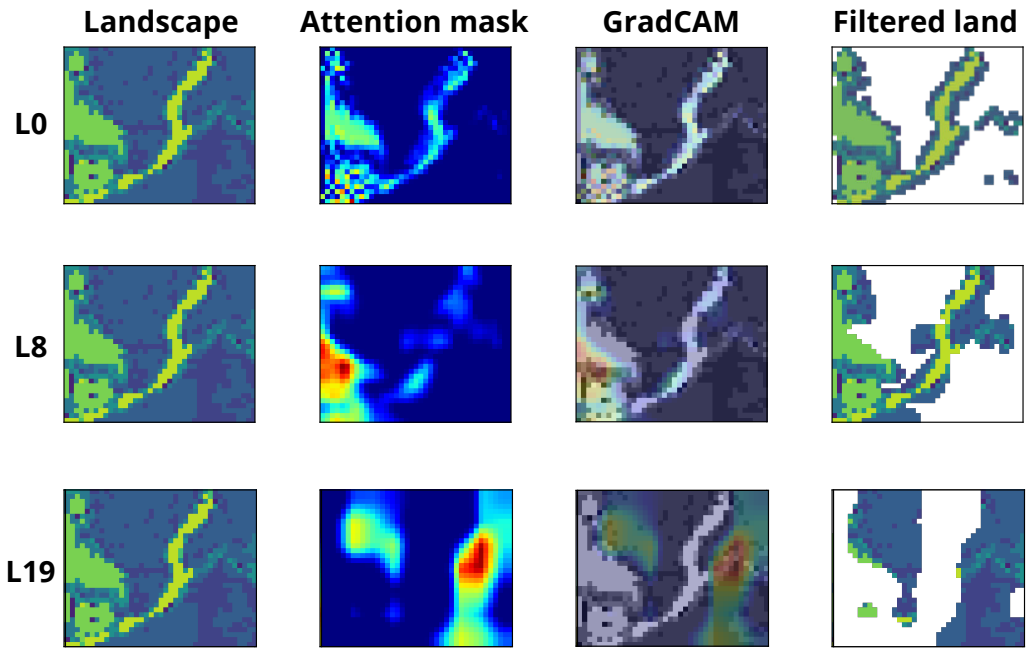

Figure 5: Zonal statistics at different layers (0, 8, and 19). Statistics are calculated by filtering the original landscapes with the attention maps/masks generated from the GradCAM algorithm, focusing the analysis on relevant regions of the landscape.

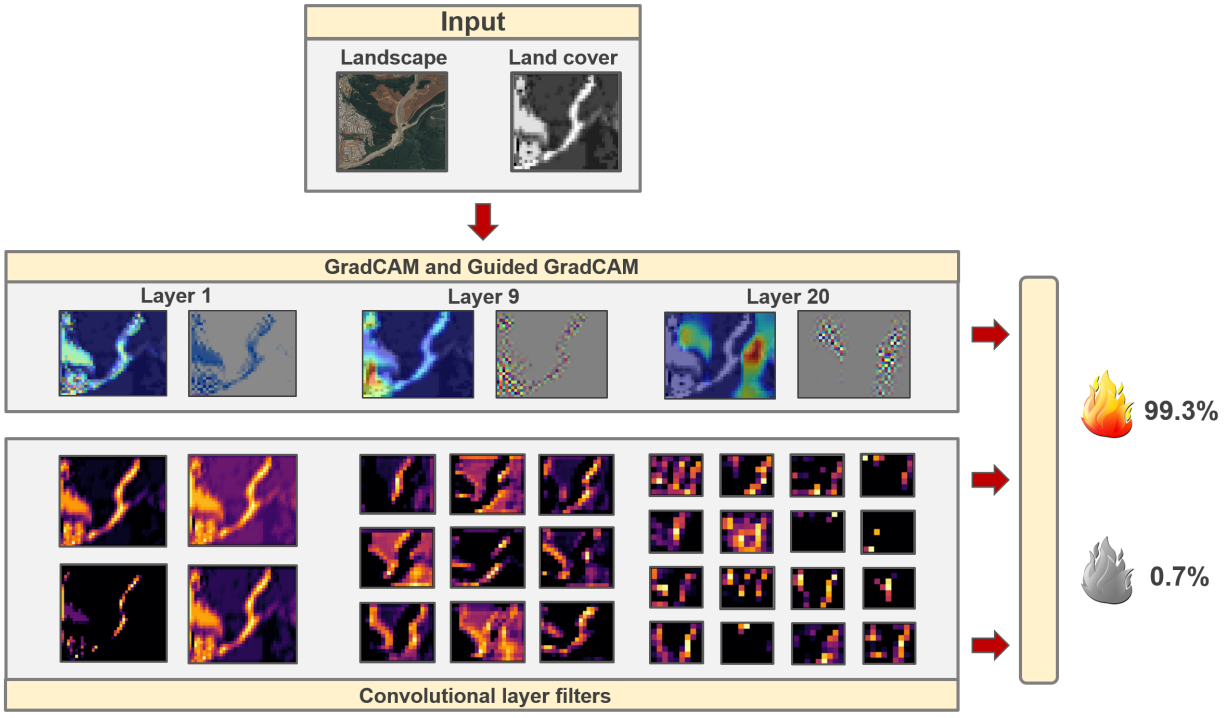

Figure 6: End-to-end classification of an example HR landscape. GradCAM, guided GradCAM, and filters visualizations are obtained at the different convolutional layers of the network to improve the interpretability of the model and open the DL black box.

Table 1: Zonal statistics. In this table, we present the statistics for high-risk (HR), medium-risk (MR), and low-risk (LR) images filtered with attention maps at different density levels. We include the total area of the landscape covered by the filter (% area heatmap), the average number of connected components (Ncomp), the sum of all values in the filtered landscape divided by Ncomp (MN), and the Simpson's diversity index to illustrate the usage of our methodology.

Attention map threshold	**Risk level**	**%Area Heatmap**	**Ncomp**	**MN**	**Simpson**
0%	HR	1	118.03	12.00	0.26
	MR	1	103.00	15.68	0.29
	LR	1	88.64	22.04	0.32
30%	HR	0.24	44.78	29.00	0.40
	MR	0.25	35.83	40.00	0.49
	LR	0.24	29.42	6.00	0.55
50%	HR	0.12	24.65	25.50	0.42
	MR	0.12	19.68	34.4	0.52
	LR	0.12	16.14	38.00	0.58
75%	HR	0.04	9.19	19.2	0.50
	MR	0.04	7.51	23.9	0.58
	LR	0.03	6.24	24.00	0.65

Table 2: Zonal statistics obtained at different layers of the model. The table summarizes the proportions of croplands (CR), native forest (NF), forest plantations (FP), grasslands (GR), shrublands (SL), and non-vegetated (NV) covers obtained from random samples of the three risk categories, filtered using the full attention maps and compared with the proportions of the original landscape. Significant variations across the layers illustrate how the network focuses its attention on specific areas of the image during the classification procedure.

Attention map filtered at 0%							
Layer	**Risk level**	**CR %**	**NF %**	**FP %**	**GR %**	**SL %**	**NV %**
0	HR	2	9	21	17	12	38
0	MR	11	9	6	25	41	4
0	LR	0	70	17	12	1	0
8	HR	2	10	28	16	10	33
8	MR	20	15	7	20	35	1
8	LR	0	67	12	21	1	0
19	HR	1	21	43	9	7	19
19	MR	28	14	4	19	29	3
19	LR	0	57	6	35	1	1
Original	HR	1	18	47	9	6	18
Original	MR	22	13	5	22	31	3
Original	LR	0	51	13	33	2	1